SCIENTIFIC REPORTS

OPEN

SUBJECT AREAS:
MATERIALS FOR ENERGY AND CATALYSIS
BATTERIES
ELECTROCHEMISTRY

Received
15 September 2014

Accepted
2 December 2014

Published
22 January 2015

Correspondence and requests for materials should be addressed to C.-M.P. (cmpark@kumoh.ac.kr)

* These authors contributed equally to this work.

Te/C nanocomposites for Li-Te Secondary Batteries

Jeong-Uk Seo[1]*, Gun-Kyu Seong[1]* & Cheol-Min Park[1,2]

[1]School of Materials Science and Engineering, Kumoh National Institute of Technology, Gumi, Gyeongbuk 730-701, Republic of Korea, [2]Outstanding Research Group Program, Convergence Technology Research Institute, Kumoh National Institute of Technology, Gumi, Gyeongbuk 730-701, Republic of Korea.

New battery systems having high energy density are actively being researched in order to satisfy the rapidly developing market for longer-lasting mobile electronics and hybrid electric vehicles. Here, we report a new Li-Te secondary battery system with a redox potential of ~1.7 V (vs. Li^+/Li) adapted on a Li metal anode and an advanced Te/C nanocomposite cathode. Using a simple concept of transforming TeO_2 into nanocrystalline Te by mechanical reduction, we designed an advanced, mechanically reduced Te/C nanocomposite electrode material with high energy density (initial discharge/charge: 1088/740 mA h cm^{-3}), excellent cyclability (ca. 705 mA h cm^{-3} over 100 cycles), and fast rate capability (ca. 550 mA h cm^{-3} at 5C rate). The mechanically reduced Te/C nanocomposite electrodes were found to be suitable for use as either the cathode in Li-Te secondary batteries or a high-potential anode in rechargeable Li-ion batteries. We firmly believe that the mechanically reduced Te/C nanocomposite constitutes a breakthrough for the realization and mass production of excellent energy storage systems.

Rechargeable Li-ion batteries are representative energy storage systems owing to their high operating voltage and relatively high energy density[1–6]. However, to satisfy the rapidly developing market for longer-lasting mobile electronic devices and hybrid electric vehicles (HEVs), much work has been devoted to finding new energy storage systems with higher energy densities than Li-ion batteries[7–13]. Among various rechargeable battery systems, rechargeable Li-sulfur (S) batteries have been proposed as an alternative system for Li-ion secondary batteries because of their high theoretical energy density of 1675 mA h g^{-1} or 3467 mA h cm^{-3} and appropriate redox potential of ~2.15 V (vs. Li^+/Li) by the reaction of $S_8 + 16Li \leftrightarrow 8Li_2S$[14–29]. Despite its advantageous features, however, the rechargeable Li-S battery is plagued by two major problems. One is the insulating characteristic of S and the other is the solubility of the Li-polysulfides generated during the discharge/charge process in various electrolytes; these problems contribute to significant loss of S during cycling and results in a poor cyclability. To solve these problems, many researchers have tried to modify S using various methods, such as fabricating S/C composites using various carbon sources, impregnating S into various conductive porous matrices, and the use of suitable electrolytes and additives[14–29]. Although these efforts have led to enhanced electrochemical performance of S electrodes, it is still not sufficient for practical utilization.

Se and Te, elements of the same group 16 in the periodic table with S, can alloy with Li to form Li_2Se and Li_2Te, respectively, which demonstrates that Se and Te may be appropriate elements to use as electrodes in rechargeable Li batteries. Recently, Se was used as a cathode material for rechargeable Li-Se batteries[30–33], in which it showed a high capacity close to its theoretical capacity (Li_2Se: 679 mA h g^{-1}). However, it exhibited a low rate capability and poor cycling behavior because of its low electrical conductivity and large volume expansion during cycling. To overcome these disadvantages, the use of Se/carbon nanocomposites prepared by various synthetic methods has been suggested as an alternative solution for enhancement of the Se electrode, such as carbon nanotube-containing Se/C and SeS_2/C composites and Se/mesoporous carbon composites[32,33]. In these nanocomposites, carbon compensates for the poor electrical conductivity of Se and accommodates its volume expansion during Li insertion/extraction. However, these Se-based composites are still not sufficient for practical utilization. Although Te has a lower theoretical gravimetric capacity (Li_2Te: 420 mA h g^{-1}) as compared with S and Se, its high density (6.24 g cm^{-3}, ca. three times higher than that of S) provides a high theoretical volumetric capacity (2621 mA h cm^{-3}). Additionally, the electronic conductivity of Te (2×10^{-4} MS m^{-1}) is considerably higher than those of S (5×10^{-22} MS m^{-1}) and Se (1×10^{-10} MS m^{-1}). Furthermore, the toxicity of Te is comparable to that of various common battery materials (LD50: Te ~5.0 g; S ~8.4 g; Co ~6.7 g; Ni ~5.0 g; Se ~6.2 g. LD50 is the individual dose required to kill 50% of a population of test animals). However, despite its advantageous features as a prospective electrode material, there are little attempts to apply Te as an electrode for Li secondary batteries.

While we are preparing this manuscript, Liu et al. have recently shown a Li-Te battery using an interesting Te/porous carbon composite by a vaccum-liquid-infusion method[34]. Although the result showed a reversible capacity of 224 mA h g^{-1} at a current rate of 50 mA g^{-1}, it showed a huge irreversible initial capacity corresponding to ca. 780 mA h g^{-1} originated from a porous carbon. Therefore, a pioneering and fundamental work for realization of Li-Te battery system is needed.

In this study, we developed a new, high-performance Li-Te secondary battery system using a Li metal anode and a Te-based cathode. Additionally, in order to overcome the problems faced when Te is used independently as a cathode material, various Te/C composites were prepared and tested for their suitability as cathode materials for the Li-Te secondary battery system. Further, a one-step reaction mechanism of Te with Li is presented on the basis of the ex situ X-ray diffraction (XRD) results along with a differential capacity plot (DCP).

Results

Electrochemical performance and reaction mechanism of Te. Figure 1a shows the voltage profiles of the Te electrode at current densities of 10 and 100 mA g^{-1}. An electrochemical test at a lower current provides near-equilibrium conditions during the galvanostatic experiment, which results in enhanced electrochemical behavior. The discharge and charge capacities of the Te electrode increased as the applied current decreased. At a current density of 100 mA g^{-1}, the Te electrode showed small discharge and charge capacities of 614 and 518 mA h cm^{-3} (156 and 132 mA h g^{-1}), respectively, whereas it showed high discharge and charge capacities of 1455 and 760 mA h cm^{-3} (370 and 193 mA h g^{-1}), respectively, at a current density of 10 mA g^{-1} (Figure 1a and S1). The Te electrodes showed very poor capacity retentions of 20.7% (current rate: 10 mA g^{-1}) and 46.1% (current rate: 100 mA g^{-1}) of the initial charge capacity after the 10th cycle, respectively. The drastic decrease in the capacity of the Te electrodes was caused by the large volume change ($\Delta V = 204\%$) due to the formation of a Li-Te alloy phase (Li_2Te), which is associated with the pulverization of the active material and its electrical isolation from the current collector. The DCP (Figure 1b) of the first cycle of the Te electrode shows a peak of 1.7 V (vs. Li^+/Li) during the discharge reaction and of 1.84 V (vs. Li^+/Li) during the charge reaction, which demonstrates that the Te electrode has a one-step reaction and a relatively high reaction potential with Li. Although the Te electrode showed a flat discharge potential of 1.7 V (vs. Li^+/Li) during the discharge reaction, its voltage profile showed a slight slope at the potential range between 1.0 and 1.5 V. To confirm the reaction at the potential range between 1.0 and 1.5 V during discharge, XRD analyses were performed. However, no structural variation was observed, which demonstrates that the reaction at the slope potential range may be related to a subreaction between the electrolyte and electrode surface. To investigate the electrochemical reaction mechanism of the Te electrode, ex situ XRD analyses were performed at fully discharged and charged states and the results are presented in Figure 1c. At the fully discharged state of 1.0 V, Te (JCPDS #36-1452, S.G.: $P3_121$, $a = 4.457$, $c = 5.927$) was fully transformed to a Li_2Te (JCPDS #23-0370, S.G.: $Fm3m$, $a = 6.517$) phase, whereas at the fully charged state of 3.0 V, the Li_2Te phase disappeared and the Te phase reappeared. On the basis of the DCP and ex situ XRD results, the following one-step electrochemical reaction mechanism of the Te electrode was revealed and the schematic representation for crystallographic transformation during cycling is shown in Figure 1d.

$$\text{During discharge: Te (hexagonal)} \rightarrow Li_2Te \text{ (cubic)}$$

$$\text{During charge: } Li_2Te \text{ (cubic)} \rightarrow \text{Te (hexagonal)}$$

Te/C nanocomposites and its electrochemical performances. The nanocomposites produced by the high energy mechanical milling (HEMM) technique were applied to Li-S and commercial Nexelion battery electrodes, both of which showed good electrochemical behaviors[15–18,32,35]. HEMM is an attractive method for fabricating high-performance electrode materials because this method yields well-distributed, nanosized metal or alloy crystallites in a carbon matrix. The HEMM plastically deforms the particles, which leads to work hardening and material fracturing upon impact at temperatures higher than 200°C and pressures on the order of 6 GPa[36]. To produce a nanocomposite containing carbon, the Te/C nanocomposite was prepared using the HEMM technique in order to enhance the electrochemical properties of the Te. The high-resolution transmission electron microscopy (HRTEM) images and XRD pattern of the Te/C nanocomposite is shown in the Figure 2a and S2. In Figure S2, all the peaks of the XRD pattern of the Te/C nanocomposite corresponded to the Te phase (JCPDS #36-1452) with reduced crystallinity because of the HEMM process. The TEM bright-field image and the HRTEM images combined with Fourier transformed (FT) patterns for the Te/C nanocomposite show that well-dispersed Te nanocrystallites with sizes of above 20 nm were contained within the amorphous carbon matrix (Figure 2a). The electrochemical properties of the Te/C nanocomposite electrode are shown in Figure 2b and c. The voltage profile (Figure 2b) of the Te/C nanocomposite electrode showed a reversible initial discharge/charge capacity of 833/613 mA h cm^{-3} (340/250 mA h g^{-1}) and a good initial Coulombic efficiency of 73.6%, values that were better than those of the Te electrode. The cycling performances of the Te and Te/C nanocomposite electrodes are compared in Figure 2c. The capacity retention of the Te/C nanocomposite electrode was 49.2% of the initial charge capacity after the 20th cycle having poor Coulombic efficiencies per cycles. Although the electrochemical performance of the Te/C nanocomposite electrode was much better than that of the Te electrode, which was still not enough for use as a cathode for Li-Te batteries.

Synthesis of mechanically reduced Te/C nanocomposite. While trying to improve the electrochemical performance of Te, we found that TeO_2 powders can be transformed to mechanically reduced Te (MR-Te) powders with reduced crystallinity by HEMM. The XRD patterns and images of the powders, which confirm the degree of MR-Te with increasing HEMM process time, are shown in Figure 3a. After HEMM for 2 h, partially reduced Te peaks appeared and the white color of the TeO_2 powder changed to a light gray color. After HEMM for 6 h, only Te peaks (JCPDS #36-1452) were observed, and the powder color was dark gray, which coincided with the Te powder. The average crystallite size of the MR-Te nanocomposite estimated using Scherrer equation was approximately 6.8 nm. On the basis of the XRD patterns and powder images, the following mechanical reduction of TeO_2 into Te was revealed:

$$TeO_2 \rightarrow \text{Te (nanocrystalline)} + O_2 \uparrow; \text{ by HEMM}$$

The mechanical reduction of TeO_2 may be related to the high pressure on the order of 6 GPa and temperature above 200°C generated during HEMM. Upon consideration of the simple mechanical reduction of TeO_2, we used this mechanical reduction method to produce a Te/C nanocomposite, and we subsequently synthesized MR-Te/C nanocomposites. The XRD pattern of the MR-Te/C nanocomposite is shown in Figure 3b. All of the XRD peaks corresponded to Te peaks (JCPDS #36-1452) and no other phases were detected. The TEM bright-field image, the HRTEM images combined with FT patterns, and the STEM image with energy dispersive spectroscopy

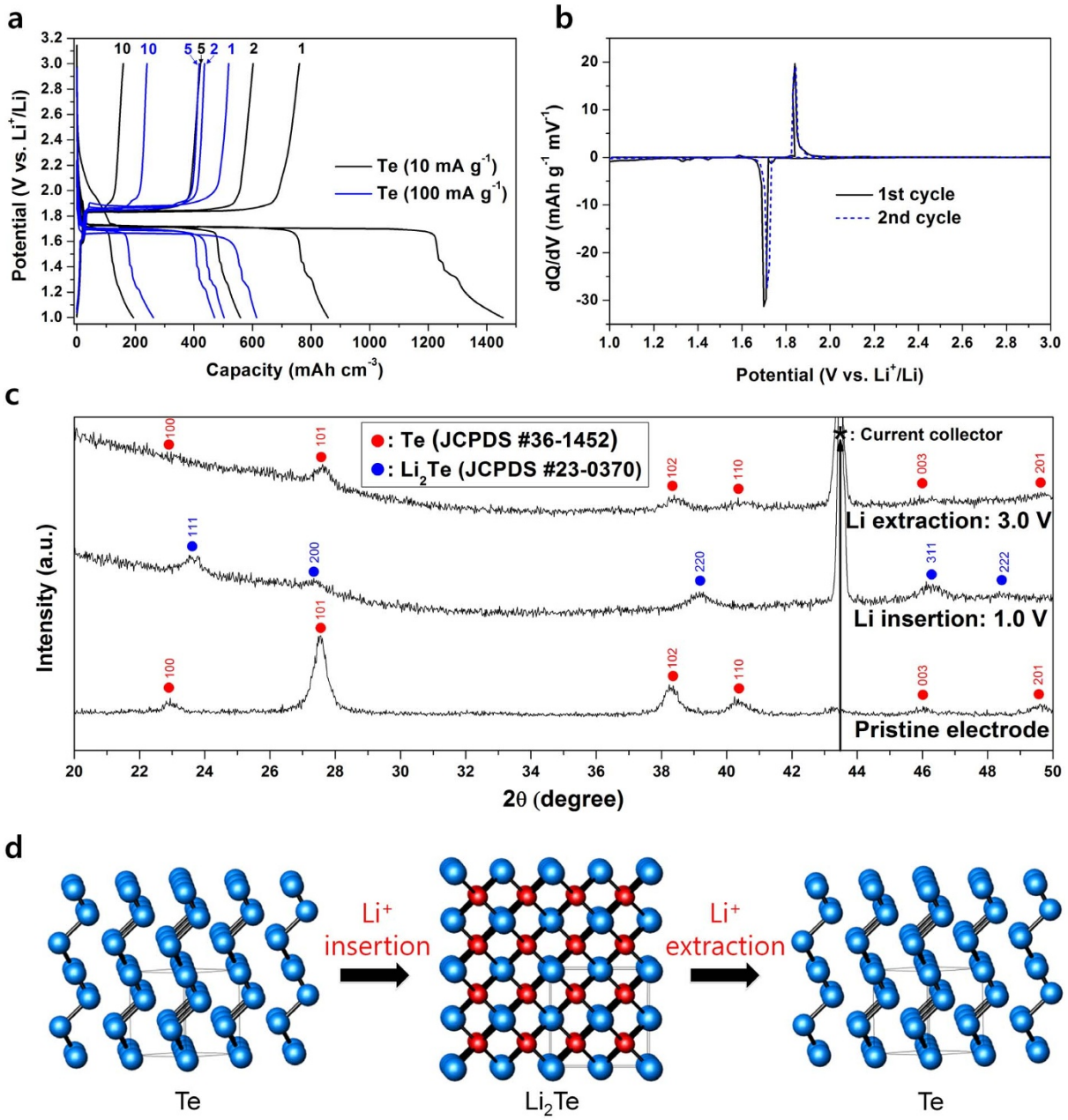

Figure 1 | Electrochemical behavior and reaction mechanism of Te electrode. (a) Voltage profile at current densities of 10 and 100 mA g^{-1}. (b) DCP of the first and second cycles. (c) Ex situ XRD results of the first cycle. (d) Schematic representation for crystallographic transformation during cycling (blue: Te atoms, red: Li atoms).

(EDS) mapping of the MR-Te/C nanocomposite show that Te nanocrystallites with sizes of approximately 5–10 nm were well dispersed within the amorphous carbon matrix (Figure 3c). Thus, it can be concluded that the MR-Te/C nanocomposite particles are composed of well-dispersed nanosized (5–10 nm) Te crystallites within the amorphous carbon matrix, as schematically illustrated in Figure 3d.

Electrochemical performances of mechanically reduced Te/C nanocomposite. To evaluate the MR-Te/C nanocomposite as a cathode material for a new Li-Te secondary battery system, the electrochemical properties of the nanocomposite were tested, and the results are shown in Figure 4 and S3. The voltage profiles of the Te and MR-Te/C nanocomposite electrodes are shown in Figure 4a (potential vs. volumetric capacity) and S3a (potential vs. gravimetric capacity), respectively. The MR-Te/C nanocomposite electrode showed a discharge potential of 1.7 V (vs. Li^+/Li) and the first discharge and charge capacities were 1088 and 740 mA h cm^{-3} (459 and 312 mA h g^{-1}), respectively, at a current density of 10 mA g^{-1}. The nanocomposite showed an excellent capacity retention of 97.4% of the initial charge capacity after the 10th cycle. However, the voltage profile of the MR-Te/C nanocomposite electrode showed a slight slope compared with those of Te electrode, which was caused by the results of the cooperated electrochemical reactions between nanocrystalline Te and ball-milled amorphous carbon and subreaction between the electrolyte and electrode surface as mentioned above. In Figure S4, the voltage profile of the ball-milled amorphous carbon electrode showed the first discharge and charge capacities of 162 and 87 mA h cm^{-3} (193 and 103 mA h g^{-1}), respectively, on the condition of the potential range between 1.0 and 3.0 V and current density of 10 mA g^{-1}. The high discharge and charge capacities of the ball-milled carbon were attributed to the degree of disordered structure and morphology and Li diffusion

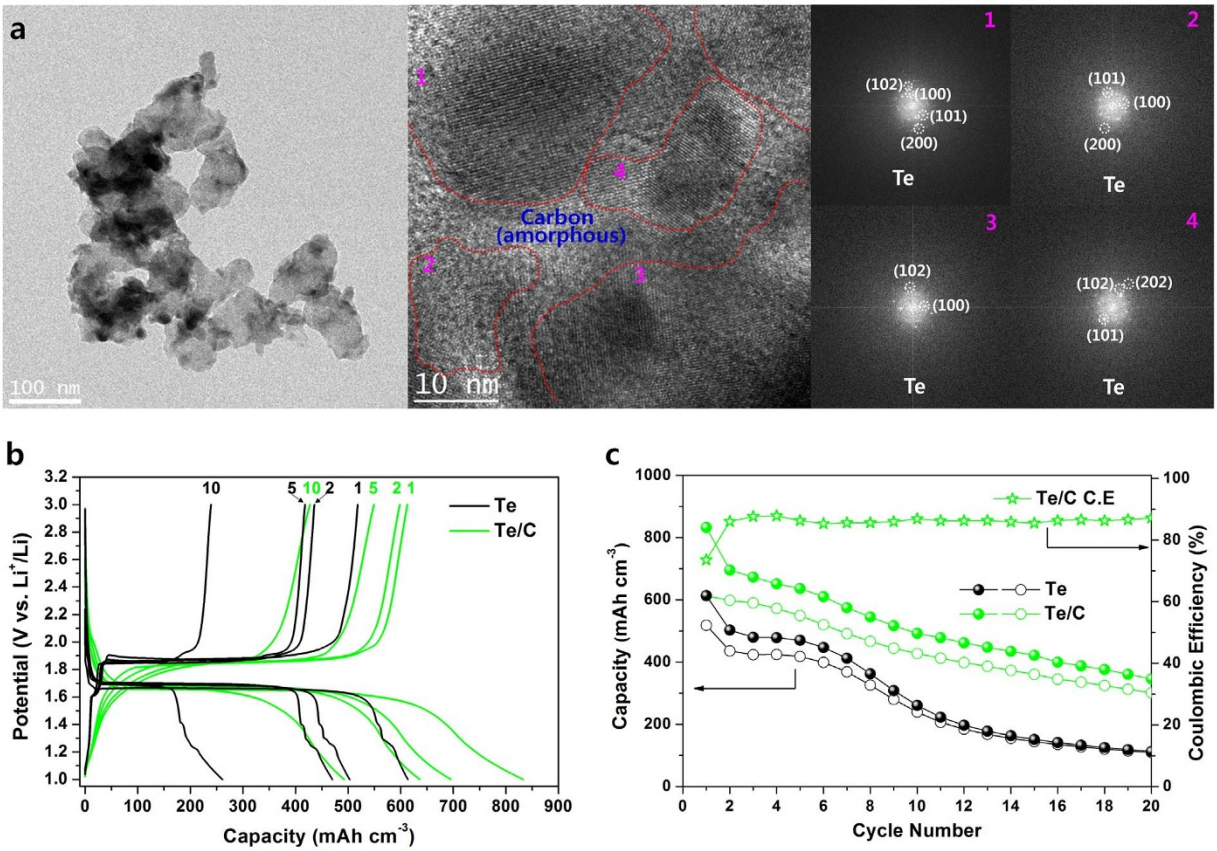

Figure 2 | Te/C nanocomposite prepared by HEMM. (a) TEM bright-field image and HRTEM images combined with FT patterns for the Te/C nanocomposite. (b) Voltage profiles of Te and Te/C nanocomposite electrodes at a current density of 10 mA g^{-1}. (c) Cycling performances of Te and Te/C nanocomposite electrodes at a cycling rate of 10 mA g^{-1}.

into the inner cores of the fractured carbons[37–39]. The first charge capacity of the ball-milled carbon (34.9 wt%) contributed in the MR-Te/C nanocomposite electrode was approximately 30 mA h cm^{-3} or 36 mA h g^{-1}. Considering the theoretical capacity of 65.1 wt% Te (273 mA h g^{-1}) and the capacity of 34.9 wt% ball-milled carbon (36 mA h g^{-1}) contributed in the MR-Te/C nanocomposite, Te in the composite electrode was fully reversible with Li, whereas the high initial discharge capacity of MR-Te/C nanocomposite was also correlated with the ball-milled carbon (corresponding to 67 mA h g^{-1}) and the subreaction between the electrolyte and electrode surface.

The MR-Te/C nanocomposite electrode showed much better electrochemical performance than the Te and Te/C nanocomposite electrodes. Comparisons of the cycling performance were made for the Te, Te/C, and MR-Te/C nanocomposite electrodes in the potential range between 1.0 and 3.0 V. The gravimetric and volumetric capacities of the Te and Te/C nanocomposite electrodes, as shown in Figure 4b and S3b, decreased gradually after a few cycles. The reversible capacity and capacity retention of the MR-Te/C nanocomposite electrode was significantly enhanced as compared to the Te and Te/C nanocomposite electrodes. The MR-Te/C nanocomposite electrode showed a very stable capacities of more than 704 mA h cm^{-3} or 297 mA h g^{-1} (current density: 10 mA g^{-1}) and 597 mA h cm^{-3} or 252 mA h g^{-1} (current density: 100 mA g^{-1}) over 100 cycles, corresponding to ca. 95% and 96% of the initial charge capacities, respectively. Additionally, the average Coulombic efficiency per cycle of the MR-Te/C nanocomposite electrode is above 99.5%. The size of the Te crystallites of the MR-Te/C nanocomposite electrode after various cycling was also analyzed using HRTEM. The HRTEM results of the samples obtained after the 10th and 50th cycles are shown in Figure S5a and b, respectively. The HRTEM images combined with FT patterns reveal the presence of the Te phase, whose crystallite size is approximately 5–10 nm after the 10th cycle, and the Te crystallites still remained 5–10 nm in size upon further cycling, even after 50 cycles. These results show that the Te nanocrystallites within the MR-Te/C nanocomposite do not agglomerate during cycling. The excellent cycling behaviour of the MR-Te/C nanocomposite electrode was attributed to the uniform distribution of 5–10-nm-sized Te crystallites within the amorphous carbon buffering matrix, which alleviated the effect of the volume expansion on the active materials, as illustrated in Figure 3d. On the basis of the results, the MR-Te/C nanocomposite can provide a new cathode material for Li-Te secondary batteries owing to its reduction potential of 1.7 V (vs. Li^+/Li) and excellent cycling behavior.

The rate capability test of the MR-Te/C nanocomposite electrode was also conducted in the potential range between 1.0 and 3.0 V. The results are shown in Figure 4c (potential vs. volumetric capacity) and 4d (volumetric capacity vs. cycle number) and in Figure S3c (potential vs. gravimetric capacity) and S3d (gravimetric capacity vs. cycle number). The figures show the cyclability of the MR-Te/C nanocomposite electrode as a function of the C rate, where C is defined as the full use of the restricted charge capacity of 700 mA h cm^{-3} in 1 h. At rates of 2C and 5C, the MR-Te/C nanocomposite electrode showed very high charge capacities of 590 and 550 mA h cm^{-3}, respectively, corresponding to ca. 79% and 75% of the charge capacity for the rate at 0.1C with stable cycling behavior. The rate capability of the MR-Te/C nanocomposite electrode was excellent, with a higher capacity than that of commercially available $Li_4Ti_5O_{12}$ anodes for Li-ion batteries. The fast rate capability of the MR-Te/C nanocomposite electrode is ascribed to the presence of the ca. 5–10-nm-sized mechanically reduced nanocrystalline Te within the amorphous carbon matrix, which contributed to short Li diffusion paths.

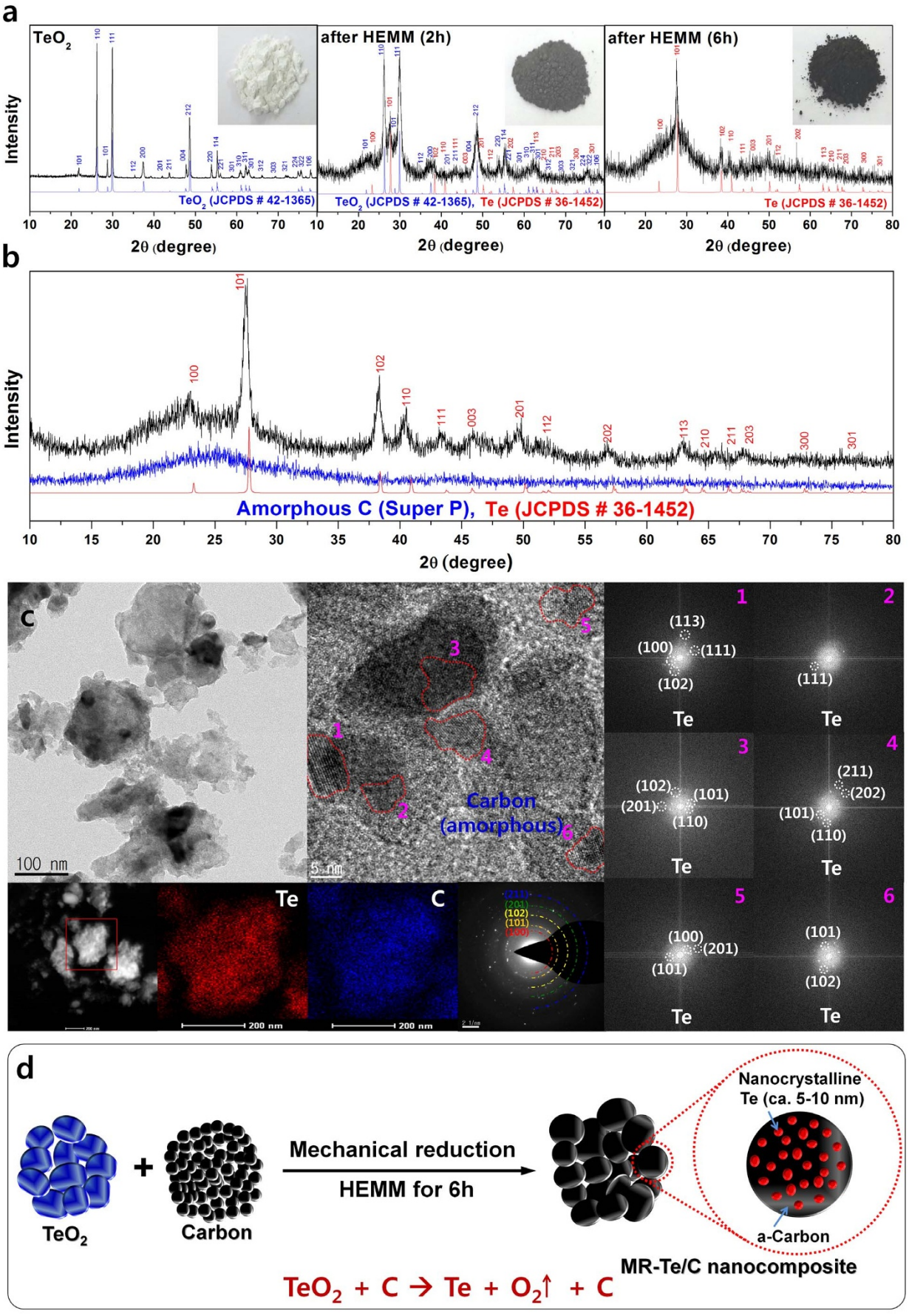

Figure 3 | **Mechanically reduced Te and its nanocomposite.** (a) XRD results and images of TeO_2 powder by HEMM at different milling times. (b) XRD pattern of the MR-Te/C nanocomposite. (c) TEM bright-field image, HRTEM images combined with FT patterns, and STEM image with EDS mapping for the MR-Te/C nanocomposite. (d) Schematic representation of MR-Te/C nanocomposite by the mechanical reduction method.

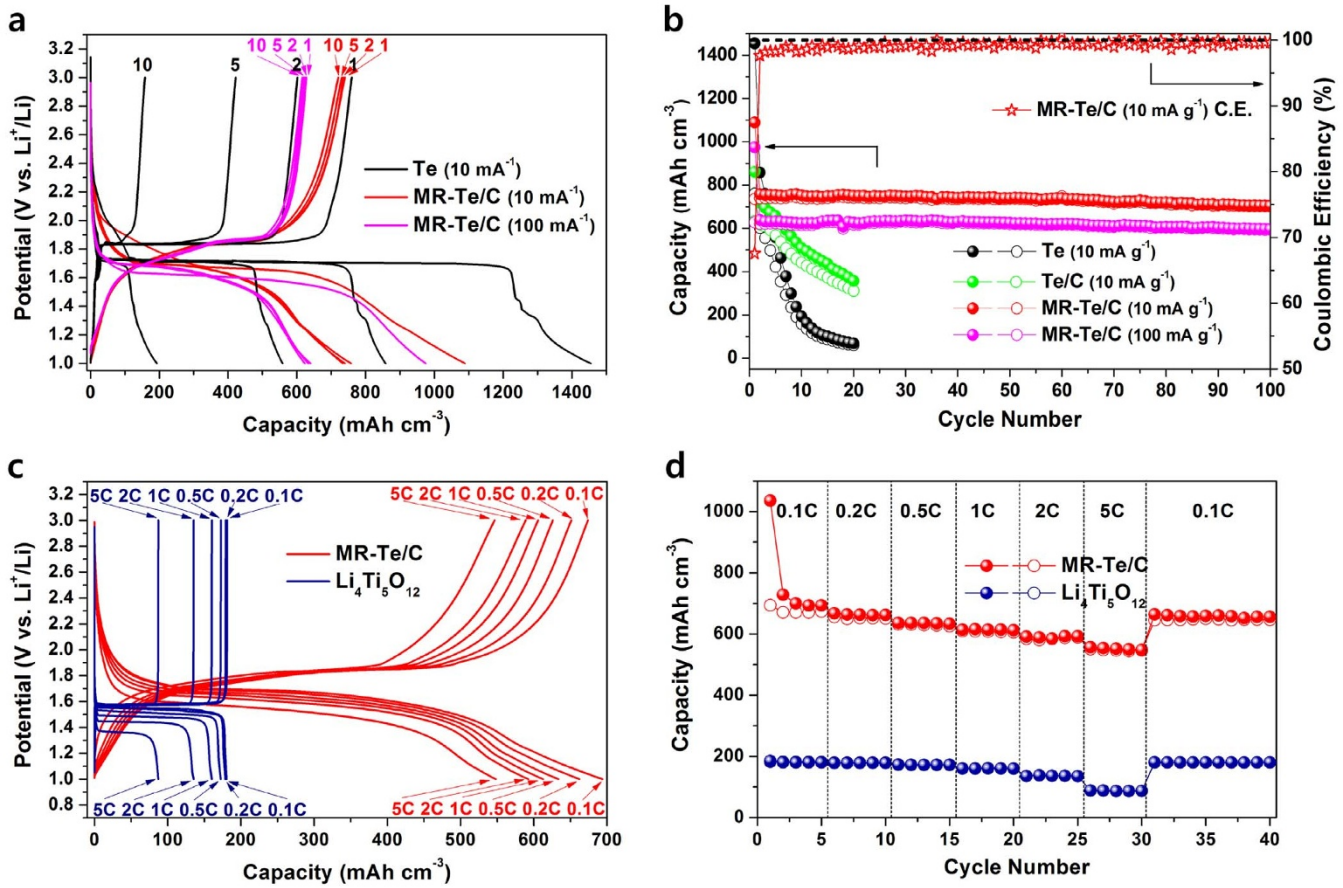

Figure 4 | Electrochemical behavior of MR-Te/C nanocomposite electrode. (a) Voltage profiles of Te (current density: 10 mA g^{-1}) and MR-Te/C nanocomposite electrodes (current density: 10 and 100 mA g^{-1}). (b) Cycling performance of Te, Te/C nanocomposite, and MR-Te/C nanocomposite electrodes at a cycling rate of 10 or 100 mA g^{-1}. (c) Voltage profiles at various C rates for $Li_4Ti_5O_{12}$ and MR-Te/C nanocomposite electrodes. (d) Plot of the discharge and charge capacity vs. cycle number for the $Li_4Ti_5O_{12}$ and MR-Te/C nanocomposite electrodes at various C rates ($Li_4Ti_5O_{12}$ - 1C: 190 mA h cm^{-3}, MR-Te/C nanocomposite - 1C: 700 mA h cm^{-3}).

Additionally, the better electrical conductivity of Te than S and Se contributed to the fast rate capability. Considering the excellent rate capability and high volumetric capacity with a reduction potential of ca. 1.7 V (vs. Li^+/Li) of the MR-Te/C nanocomposite electrode, it can be utilized as either the cathode in Li-Te secondary batteries or a high-potential anode in rechargeable Li-ion batteries.

Discussion

By introducing a new materials pair into a secondary battery system, we have successfully developed a stable Li-Te secondary battery system with excellent electrochemical performances. Specifically, we adopted a Li metal anode and a MR-Te/C nanocomposite cathode, which are stable materials, achieving a redox potential of ~1.7 V (vs. Li^+/Li). Using a simple and interesting concept of transforming TeO_2 into nanocrystalline Te by mechanical reduction, the MR-Te/C nanocomposite was synthesized and applied as a high-performance cathode in Li-Te secondary batteries. Additionally, the MR-Te/C nanocomposite can be utilized as a high-potential anode in rechargeable Li-ion batteries. The advantageous features of the MR-Te/C nanocomposite are as follows. First, when the MR-Te/C nanocomposite was applied as a cathode material in a new Li-Te secondary battery, it showed a relatively high redox potential of ~1.7 V (vs. Li^+/Li), high energy density (initial discharge/charge: 1088/740 mA h cm^{-3}), excellent cyclability (ca. 705 mA h cm^{-3} over 100 cycles), and fast rate capability (ca. 550 mA h cm^{-3} at 5C rate). Second, because the MR-Te/C nanocomposite electrode showed a better rate capability and higher energy density than commercially available $Li_4Ti_5O_{12}$ anodes, the MR-Te/C nanocomposite can be used as a high-potential anode for rechargeable Li-ion batteries. Third, as demonstrated on the basis of the DCP and ex situ XRD results, the one-step electrochemical reaction mechanism of the Te electrode with Li provides a stable battery system unlike rechargeable Li-S battery forming various soluble Li-polysulfides generated during the discharge/charge process in various electrolytes.

In summary, we have developed a simple mechanical reduction method of transforming TeO_2 into nanocrystalline Te using a high-energy mechanical milling technique at ambient temperature and pressure. Further modification with carbon produced a MR-Te/C nanocomposite that, when applied as a cathode material for a new Li-Te rechargeable batteries, showed excellent cycling performance with high volumetric capacities. Additionally, the MR-Te/C nanocomposite electrode showed excellent rate capabilities with high volumetric capacities, which proves that it is very applicable to high potential anodes with $Li_4Ti_5O_{12}$. We anticipate that the MR-Te/C nanocomposite will pave the way for the realization and mass production of excellent energy storage systems.

Methods

Sample Preparation. Te/C nanocomposite was prepared using Te (Aldrich, 99.98%, average size ca. 50 μm) and carbon (Super P, Timcal) powders. The powders were prepared by HEMM (Spex-8000) at ambient temperature and pressure as follows: the powders were placed into an 80 cm^3 hardened steel vial with stainless steel balls (diameter: 3/8 in. and 3/16 in.) at a ball-to-powder ratio of 20 : 1. The HEMM process was carried out under an Ar atmosphere for 6 h. Preliminary studies showed that the optimum composition was 70 wt% Te to 30 wt% carbon. Mechanically reduced Te was synthesized by the same HEMM technique using a TeO_2 powder (Aldrich,

>99%, average size ca. 20 μm). To synthesize the mechanically reduced Te/C nanocomposite, the same HEMM technique was employed to mill mixtures of the TeO_2 and carbon powders. Preliminary electrochemical tests revealed that, in terms of the electrochemical performance such as initial capacity, initial coulombic efficiency, and cycle performance, the optimum amounts were 70 wt% TeO_2 and 30 wt% C, which correspond to the exact composition of 65.1 wt% Te and 34.9 wt% C within the mechanically reduced Te/C nanocomposite.

Materials Characterization. To observe the structural changes in the active material of the Te electrode during cycling, ex situ XRD (DMAX2500-PC, Rigaku) analyses were used. The Te/C and mechanically reduced Te/C nanocomposites were characterized using XRD, HRTEM (FEI F20, operating at 200 kV), and EDS (attached to the HRTEM).

Electrochemical Measurements. For the electrochemical evaluation of Te, Te/C, and mechanically reduced Te/C nanocomposites, test electrodes consisting of the active powder (70 wt%), carbon black (Denka, 15 wt%) as a conducting agent, and polyvinylidene fluoride (PVDF, 15 wt%) dissolved in N-methyl-2-pyrrolidone (NMP) as a binder were fabricated. Samples of each mixture were vacuum-dried at 120°C for 3 h and pressed (electrode thickness: ca. 0.045 mm, electrode area: 0.79 cm^2, weight of active material: ca. 2.5 mg). Coin-type electrochemical cells were assembled in an Ar-filled glove box using a Celgard 2400 separator, Li foil as the counter and reference electrodes, and 1 M $LiPF_6$ in ethylene carbonate/diethyl carbonate (EC/DEC, 1 : 1 by volume, Panax STARLYTE) as the electrolyte. All the cells were tested galvanostatically between 1.0 and 3.0 V (vs. Li^+/Li) at current densities of 10 and 100 mA g^{-1} using a Maccor automated tester except the rate capability tests. The gravimetric capacity was calculated on the basis of the weight of the active materials, and the volumetric capacity was calculated by multiplying the gravimetric capacity by the tap density (Te: 3.93 g cm^{-3}, Te/C: 2.45 g cm^{-3}, mechanically reduced Te/C: 2.37 g cm^{-3}, $Li_4Ti_5O_{12}$: 1.11 g cm^{-3}, ball-milled amorphous carbon: 0.84 g cm^{-3}), which was measured using a powder tap density tester (BT-301, Bettersize). Li was inserted into the electrode during the discharge reaction and was extracted from the working electrode during the charge reaction.

1. Park, C.-M., Kim, J.-H., Kim, H. & Sohn, H.-J. Li-alloy based anode materials for Li secondary batteries. *Chem. Soc. Rev.* **39**, 3115–3141 (2010).
2. Winter, M., Besenhard, J. O., Spahr, M. E. & Novak, P. Insertion electrode materials for rechargeable lithium batteries. *Adv. Mater.* **10**, 725–763 (1998).
3. Marom, R., Amalraj, S. F., Leifer, N., Jacob, D. & Aurbach, D. A review of advanced and practical lithium battery materials. *J. Mater. Chem.* **21**, 9938–9954 (2011).
4. Cabana, J., Monconduit, L., Larcher, D. & Palacin, M. R. Beyond intercalation-based Li-ion batteries: The state of the art and challenges of electrode materials reacting through conversion reactions. *Adv. Energy Mater.* **22**, E170–E192 (2010).
5. Larcher, D. *et al.* Recent findings and prospects in the field of pure metals as negative electrodes for Li-ion batteries. *J. Mater. Chem.* **17**, 3759–3772 (2007).
6. Etacheri, V., Marom, R., Elazari, R., Salitra, G. & Aurbach, D. Challenges in the development of advanced Li-ion batteries: a review. *Energy & Environ. Sci.* **4**, 3243–3262 (2011).
7. Kim, H. *et al.* Metallic anodes for next generation secondary batteries. *Chem. Soc. Rev.* **42**, 9011–9034 (2013).
8. Bruce, P. G., Freunberger, S. A., Hardwick, L. J. & Tarascon, J.-M. Li-O_2 and Li-S batteries with high energy storage. *Nat. Mater.* **11**, 19–29 (2012).
9. Choi, N. S. *et al.* Challenges facing lithium batteries and electrical double-layer capacitors. *Angew. Chem. Int. Ed.* **51**, 9994–10024 (2012).
10. Lu, J. *et al.* A nanostructured cathode architecture for low charge overpotential in lithium-oxygen batteries. *Nat. Commun.* **4**, 2383 (2013).
11. Girishkumar, G., McCloskey, B., Luntz, A. C., Swanson, S. & Wilcke, W. Lithium air battery: promise and challenges. *J. Phys. Chem. Lett.* **1**, 2193–2203 (2010).
12. Yoo, H. *et al.* Mg rechargeable batteries: an on-going challenge. *Energy Environ. Sci.* **6**, 2265–2279 (2013).
13. Slater, M. D., Kim, D., Lee, E. & Johnson, C. S. Sodium-ion batteries. *Adv. Funct. Mater.* **23**, 947–958 (2013).
14. Yang, Y. *et al.* High-capacity micrometer-sized Li_2S particles as cathode materials for advanced rechargeable lithium-ion batteries. *J. Am. Chem. Soc.* **134**, 15387–15394 (2012).
15. Manthiram, A., Fu, Y. & Su, Y. S. Challenges and prospects of lithium-sulfur batteries. *Acc. Chem. Res.* **46**, 1125–1134 (2013).
16. Evers, S. & Nazar, L. F. New approaches for high energy density lithium-sulfur battery cathodes. *Acc. Chem. Res.* **46**, 1135–1143 (2013).
17. Yang, Y., Zheng, G. & Cui, Y. Nanostructured sulfur cathodes. *Chem. Soc. Rev.* **42**, 3018–3032 (2013).
18. Ji, X. & Nazar, L. F. Advances in Li-S batteries. *J. Mater. Chem.* **20**, 9821–9826 (2010).
19. Li, W. *et al.* Understanding the role of different conductive polymers in improving the nanostructured sulfur cathode performance. *Nano Lett.* **13**, 5534–5540 (2013).
20. Chen, H. *et al.* Ultrafine sulfur nanoparticles in conducting polymer shell as cathode materials for high performance lithium/sulfur batteries. *Sci. Rep.* **3**, 1910 (2013).
21. Su, Y.-S. & Manthiram, A. Lithium-sulphur batteries with a microporous carbon paper as a bifunctional interlayer. *Nat. Commun.* **3**, 1166 (2012).
22. Schuster, J. *et al.* Spherical ordered mesoporous carbon nanoparticles with high porosity for lithium-sulfur batteries. *Angew. Chem. Int. Edit.* **51**, 3591–3595 (2012).
23. She, Z. W. *et al.* Sulphur–TiO_2 yolk–shell nanoarchitecture with internal void space for long-cycle lithium–sulphur batteries. *Nat. Commun.* **4**, 1331 (2013).
24. Mikhaylik, Y. V. & Akridge, J. R. Polysulfide shuttle study in the Li/S battery system. *J. Electrochem. Soc.* **151**, A1969–A1976 (2004).
25. Ji, X., Lee, K. T. & Nazar, L. F. A highly ordered nanostructured carbon-sulphur cathode for lithium-sulphur batteries. *Nat. Mater.* **8**, 500–506 (2009).
26. Elazari, R., Salitra, G., Garsuch, A., Panchenko, A. & Aurbach, D. Sulfur-impregnated activated carbon fiber cloth as a binder-free cathode for rechargeable Li-S batteries. *Adv. Mater.* **23**, 5641–5644 (2011).
27. Zheng, G., Yang, Y., Cha, J. J., Hong, S. S. & Cui, Y. Hollow carbon nanofiber-encapsulated sulphur cathodes for high specific capacity rechargeable lithium batteries. *Nano Lett.* **11**, 4462–4467 (2011).
28. Jayaprakash, N., Shen, J., Moganty, S. S., Corona, A. & Archer, L. A. Porous hollow carbon@sulphur composites for high-power lithium-sulphur batteries. *Angew. Chem. Int. Ed.* **50**, 5904–5908 (2011).
29. Xiao, L. *et al.* A soft approach to encapsulate sulphur: polyaniline nanotubes for lithium-sulphur batteries with long cycle life. *Adv. Mater.* **24**, 1176–1181 (2012).
30. Liu, L. *et al.* Nanoporous selenium as a cathode material for rechargeable lithium–selenium batteries. *Chem. Commun.* **49**, 11515–11517 (2013).
31. Kwon, H.-T. & Park, C.-M. Electrochemical characteristics of ZnSe and its nanostructured composite for rechargeable Li-ion batteries. *J. Power Sources* **251**, 319–324 (2014).
32. Abouimrane, A. *et al.* A new class of lithium and sodium rechargeable batteries based on selenium and selenium−sulfur as a positive electrode. *J. Am. Chem. Soc.* **134**, 4505–4508 (2012).
33. Luo, C. *et al.* Selenium@mesoporous carbon composite with superior lithium and sodium storage capacity. *ACS nano* **7**, 8003–8010 (2013).
34. Liu, Y. *et al.* Lithium-tellurium batteries based on tellurium/porous carbon composite. *J. Mater. Chem. A* **2**, 12201–12207 (2014).
35. Ishihara, H., Mizutani, S. & Inoue, H. inventors; SONY Corporation, assignee. Anode active material and battery using the same. *United States patent* US 11/268,010. 2005 Nov 7.
36. Suryanarayana, C. Mechanical alloying and milling. *Prog. Mater. Sci.* **46**, 1–184 (2001).
37. Xing, W., Dunlap, R. A. & Dahn, J. R. Studies of lithium insertion in ball-milled sugar carbons. *J. Electrochem. Soc.* **145**, 62–70 (1998).
38. Wang, C. S., Wu, G. T. & Li, W. Z. Lithium insertion in ball-milled graphite. *J. Power Sources* **76**, 1–10 (1998).
39. Gao, B. *et al.* Enhanced saturation lithium composition in ball-milled single-walled carbon nanotubes. *Chem. Phys. Lett.* **327**, 69–75 (2000).

Acknowledgments

This research was supported by the MSIP (Ministry of Science, ICT and Future Planning), Korea, under the "Creative ICT Convergence Human Resource Development" support program (NIPA-2014-H7501-14-1002) supervised by NIPA (National IT Industry Promotion Agency).

Author contributions

C.-M.P. initiated the idea and outlined the experiments. J.-U.S. and G.-K.S. synthesized samples and performed various analyses. C.-M.P. supervised the research work and wrote the manuscript. All authors contributed to discussion on the results for the manuscript.

Additional information

Supplementary information accompanies this paper at http://www.nature.com/scientificreports

Competing financial interests: The authors declare no competing financial interests.

How to cite this article: Seo, J.-U., Seong, G.-K. & Park, C.-M. Te/C nanocomposites for Li-Te Secondary Batteries. *Sci. Rep.* **5**, 7969; DOI:10.1038/srep07969 (2015).